JOURNAL OF CATALYSIS 152, 147–163 (1995)

Solid Electrolyte Potentiometric Study of La(Sr)MnO_3 Catalyst during Carbon Monoxide Oxidation

P. D. Petrolekas and I. S. Metcalfe[1]

Department of Chemical Engineering and Chemical Technology, Imperial College of Science, Technology and Medicine, London SW7 2BY, United Kingdom

Received April 27, 1994; revised August 3, 1994

The catalytic behaviour of the perovskite oxide $La_{0.5}Sr_{0.5}MnO_{3-\delta}$ was investigated during carbon monoxide oxidation at 500–550°C. The technique of solid electrolyte potentiometry was employed to monitor the oxygen activity of the solid catalyst under reaction conditions. At 550°C, the reaction rate was found to be a function of the gas phase oxygen (or carbon monoxide) partial pressure and the catalyst oxygen activity. At 500°C, the rate tended to depend only on the gas phase composition and not on the catalyst state. The results suggested that the reaction mechanism changes from an *ionic* redox model (550°C), where the reoxidation of the reduced sites occurs by lattice oxygen, to a Mars–van Krevelen redox model (500°C), where the reoxidation occurs by gas phase oxygen. The hysteresis at 550°C was attributed to diffusional limitations appearing during either the reoxidation of the reduced sites or the reoxidation of the oxide bulk. The change in the reaction mechanism in going from 500 to 550°C was considered to be the result of an increase in the mobility of lattice oxygen, in agreement with the oxygen temperature programmed desorption profile of the catalyst.

INTRODUCTION

Solid electrolyte potentiometry (SEP) is a technique whereby the oxygen activity of a catalyst is determined *in situ* by measuring the emf of a solid-state electrochemical cell. The cell typically consists of an O^{2-} conducting membrane separating reference and reaction compartments. The catalyst is in the form of a porous electrode film deposited on the electrolyte (e.g., yttria-stabilized zirconia, YSZ). The technique of SEP has been employed in a number of fundamental studies on metal catalysts and has been reviewed in detail (1–3). The measurement of the activity of adsorbed oxygen species under reaction conditions has proved to be very useful in understanding the reaction mechanism.

So far, SEP has not been widely used on metal oxide catalysts. This is partly because only a limited number of oxide materials exhibit high electronic conductivity and, at the same time, good thermal and chemical compatibility with the electrolyte. Attempts to overcome these limitations have been made by using oxide-covered metal electrodes. Breckner *et al.* (4) used a platinum electrode covered with a vanadium phosphate oxide (VPO) catalyst for the oxidation of butene. However, in this case, the underlying metal may have been in contact with the gas phase, and therefore the catalytic and the electrocatalytic reactions will also take place on the metal. Average, rather than uniform, rate and oxygen activity values may be then measured.

A fundamental difference between metal and oxide electrodes lies in the fact that metals are pure electronic conductors, while oxides are mixed conducting materials. The electrocatalytic reaction at metal/YSZ electrodes takes place at the three-phase boundary line, where oxygen is reduced and incorporated in the electrolyte (1–3). To the extent that this is the only charge transfer reaction, the emf of the cell measures the activity of adsorbed oxygen species. However, the charge transfer reaction can follow a different pathway at an oxide/YSZ electrode. Oxygen can be reduced at the oxide surface, diffuse through the lattice to the oxide/YSZ interface, and then transfer to the electrolyte. If this is the operating charge transfer reaction, then the emf need not reflect the activity of adsorbed oxygen but will reflect the activity of lattice oxygen species in the oxide bulk.

Recently Hildenbrand and Lintz (5, 6) presented SEP measurements on a copper oxide electrode catalyst during the partial oxidation of propene to acrolein. They suggested that the potentiometric oxygen activity is a measure of the oxygen in the bulk of the solid catalyst (i.e., the oxidation state). The relation between the different phases of the solid catalyst (CuO, Cu_2O, Cu) formed under working conditions, and the selectivity of the reaction was accordingly examined. It was confirmed that the acrolein formation occurs mainly in the domain where copper(I) oxide is stable.

[1] E-mail: I.Metcalfe@ic.ac.uk.

0021-9517/95 $6.00

Breckner *et al.* (4) also suggested that the SEP oxygen activity is a bulk quantity. Accordingly, they attributed changes in the selectivity of butene oxidation to the phase transitions of the solid VPO catalyst. However, in this particular case, the exchange of oxygen between the surface and the bulk was in equilibrium and, hence, the emf would be expected to reflect the common activity of surface and bulk oxygen species.

In this work, SEP is used to monitor the oxygen activity of a perovskite-type oxide $La_{0.5}Sr_{0.5}MnO_{3-\delta}$ catalyst during high-temperature (500–550°C) CO oxidation. The perovskites ABO_3 have attracted attention since they were found to be efficient catalysts for the oxidation of CO, the reduction of NO_x, and the complete oxidation of light hydrocarbons (C_1–C_4) (7, 8). Furthermore, because of high electronic and ionic conductivities, perovskites constitute some of the most promising electrode materials for solid oxide fuel cells (9, 10). Emphasis has been given to Sr-doped $LaMnO_3$ since it exhibits high electronic (positive hole) conductivity, good compatibility with the YSZ electrolyte, and high activity for the reduction of oxygen (10–12).

Apart from practical applications, perovskite-type oxides $ABO_{3-\delta}$ have a major theoretical interest. They offer the possibility to control the valence state of the transition metal B and the oxygen nonstoichiometry δ by partial substitution in the A or B position. The stability of the perovskite structure for a wide variety of compositions allows the study of the relationship between defect structure and catalytic activity in such a series of isostructural materials (13–15).

Voorhoeve *et al.* (8) introduced the terms suprafacial and intrafacial catalysis in order to characterize the behaviour of a series of perovskite-type oxide catalysts. Suprafacial processes are considered to be low-temperature processes proceeding through reactions with adsorbed species. Conversely, intrafacial or high-temperature processes involve the removal and incorporation of lattice oxygen of the oxide. The relative importance of the two processes has been previously examined during the oxidation of methane on $La_{1-x}Sr_xMnO_3$ catalyst (16).

In this work, it will be shown that the technique of SEP is particularly useful in studying the mechanism of the intrafacial reaction for CO oxidation on $La(Sr)MnO_{3-\delta}$.

EXPERIMENTAL METHODS

Apparatus

The solid-state electrochemical cell used in this study was the following:

$$\text{air, Pt}\,|\,ZrO_2, 8\%Y_2O_3\,|\,La_{0.5}Sr_{0.5}MnO_3, O_2, CO, CO_2, N_2. \quad [1]$$

The working $La_{0.5}Sr_{0.5}MnO_3$ electrode was exposed to reaction conditions and served simultaneously as the catalyst for the reaction under study. The reference platinum electrode was exposed to air, $P_{O_2,R} = 0.21$. The electrode potential difference, i.e., the emf of the cell, was monitored by means of a DD10M Potentiostat/Galvanostat (Sycopel Scientific).

The electrochemical reactor setup has been described in detail elsewhere (17). The cell was in the form of a YSZ thimble, with an internal painted Pt electrode and two external ring electrodes made of the perovskite catalyst. The projected areas of the two oxide electrodes were 3.0 and 0.3 cm^2, respectively (the small electrode was made to serve as the unpolarized reference electrode in closed-circuit operation). Gold leads (Engelhard Ind., Ltd.) were mechanically attached to the electrodes. The reactor, made of aluminium, was placed in a box furnace (Gallenkamp Ind.) equipped with a temperature controller.

The zero grade air, CO/N_2, and N_2 gases (BOC Special Gases) were regulated and purified (Alltech Assoc., Inc.). Air was passed over the internal electrode at all times, with a flowrate of 50 sccm. A recycle pump (Charles Austen Pumps, Ltd.) was used to ensure that the reactor behaviour remained close to that of a CSTR. The net flowrate through the reaction side was 230 sccm, while in the recycle loop the flowrate was 10 times higher. The pressure in the recycle reactor was 1.65 bar.

A Binos 100 non-dispersive infrared photometer (Rosemount) was placed in the reactor outlet stream to analyze carbon monoxide and carbon dioxide continuously (the time response of the IR analyzer was of the order of a few seconds). A bypass system was constructed for the reactant stream composition to be analyzed and mass balances to be verified.

The oxygen in the outlet stream was analyzed only during calibration procedures and occasionally during experimental runs. This was done by means of a gas chromatograph (Pye 104), fitted with a column of molecular sieve 5A. The TCD signals were collected and integrated by means of PU4820 Chromate Data System (Philips) software installed on an Amstrad PC3386 SX.

The overall conversion of CO to CO_2 was in most cases less than 10%. At constant gas phase composition, the rate was found to be independent of the total flowrate, indicating that external mass transfer limitations were not important. Runs in the absence of catalyst showed that no appreciable homogeneous reactions occurred.

The highest reaction temperature employed (550°C) was well below that of the explosion limit for CO/O_2 reaction at the composition and pressure used (18). However, for reasons of safety, flame arrestors were placed immediately upstream and downstream of the reactor and the volume of the reactor section was minimized.

Catalyst

The $La_{0.5}Sr_{0.5}MnO_3$ oxide material was prepared by the solid-state diffusion process, using high-purity oxide precursor powders obtained from Aldrich Chem., Ltd. The appropriate proportions were mixed and calcined to form the catalyst powder. The X-ray diffraction spectrum of the material showed the presence of the single perovskite phase.

The oxide electrodes were made according to the tape-casting slurry technique; 100 g of the perovskite powder was added to a mixture of 15 g binder (polyvinylbutyral), 7.5 g plasticizer (1 : 1 mixture of polyethylene glycol 400 and dibutyl phthalate) and 60 cm^3 solvent (ethanol). Drops of a dispersing agent (fish oil) were added, and the slurry was homogenized. The film electrodes were made by spreading the slurry over the YSZ electrolyte thimbles and sintering in air at 1275°C for 2 h.

The experiments were performed over two similar $La_{0.5}Sr_{0.5}MnO_3$ electrodes, namely A and B. They were both prepared using the same oxide powder and following the procedure described above. The surface areas of the perovskite samples were determined by BET measurements using krypton. The surface area of the fresh perovskite powder was 0.26 m^2/g. The surface areas of the oxide electrode-painted YSZ thimbles were measured after reaction (the experiments were carried out over a period of several months on each electrode). They were found to be $S_A = 98 \pm 3$ cm^2 and $S_B = 232 \pm 3$ cm^2 for electrodes A and B, respectively. The surface area of the YSZ thimble alone was about 5 cm^2.

The XPS spectrum of the A-$La_{0.5}Sr_{0.5}MnO_3$/YSZ electrode showed the presence of a large amount of carbon on the catalyst surface (19); this was probably due to the organic compounds used in the electrode preparation. The oxide electrode was also examined after reaction. A carbon peak of similar intensity was observed, indicating that in the temperature range of the investigation (500–550°C) carbon was not deposited on or removed from the oxide surface. A decrease in the relative intensity of the oxygen peak of the used sample was also noted. Possible variations in the surface concentrations of the other components could not be identified.

Scanning electron microscopy (SEM) photographs of the fresh and used $La_{0.5}Sr_{0.5}MnO_3$/YSZ electrode samples showed that the average particle size of the porous oxide was 3–5 μm. No significant differences between the two samples were noted.

The Nernstian behaviour of the oxide electrode was examined by introducing O_2/N_2 gas mixtures of known compositions to the cell at 500°C. The emf values obtained were within 1–2 mV agreement with those predicted by the Nernst equation, indicating the proper electrode behaviour of the oxide material (high electronic conductivity and good electrode-electrolyte adherence).

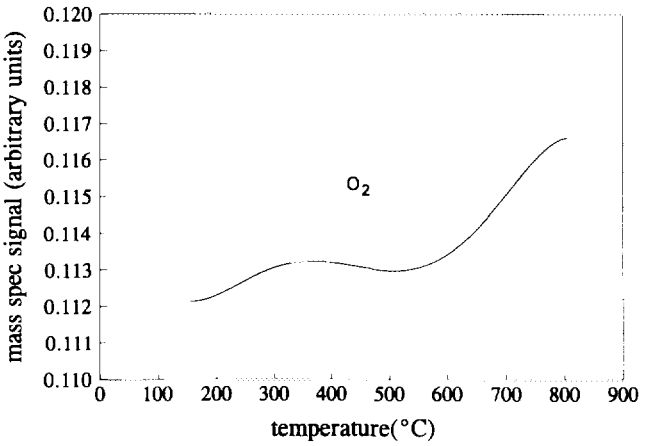

FIG. 1. Temperature programmed desorption of oxygen from $La_{0.5}Sr_{0.5}MnO_3$; heating rate = 10°C/min.

Temperature programmed desorption (TPD) and reduction (TPR) experiments were performed on the $La_{0.5}Sr_{0.5}MnO_3$ powder using a purpose-built apparatus (20). The TPD profile of oxygen was obtained as follows. Initially, a fresh perovskite sample (76.1 mg) was preoxidized at 500°C for 1 h in an atmosphere of 20% O_2 in helium. Then, the system was cooled to room temperature, flushed with pure helium, and heated. The temperature was ramped linearly at a rate of 10°C/min up to 800°C. The TPD "spectrum" is presented in Fig. 1. Two oxygen peaks are shown. The first one is present at low temperatures, while the second one begins at temperatures just above 500°C. Following the identification of TPD peaks proposed by Yamazoe and Teraoka (14), the low-temperature peak is referred to as α-oxygen and the high-temperature peak as β-oxygen. Taking the surface area occupied by one oxygen atom as 0.07 nm^2, the coverage of α-oxygen species can be calculated to be 0.92.

The TPR experiments were carried out using either carbon monoxide or hydrogen as the reducing agent. The oxide was heated to 900°C at a rate of 10°C/min. Two main peaks appeared in both TP reductions, the first at 620°C (CO-TPR) or 650°C (H_2-TPR) and the second at 770–780°C. In both cases the oxide was reduced up to $3 - \delta = 2.40$–2.45, i.e., 1.1–1.2 e^-/molecule (19).

RESULTS

The steady-state experiments were carried out at 500 and 550°C. The procedure involved keeping the partial pressure of one of the reactants constant, O_2 or CO, and varying the other, CO or O_2, respectively. In all cases, cyclic variations were performed. During an O_2-cycle the gas phase concentration of CO was constant at 6%, while the concentration of O_2 varied in the range of 2–16%. The

CO-cycles were performed at 5% O_2 and 2–16% CO. The emf, E, of the solid-state electrochemical cell was continuously measured in order to determine the oxygen activity of the catalyst, α_O, under reaction conditions. The simultaneous recording of the outlet carbon dioxide concentration, y_{CO_2}, by means of IR spectrometry, allowed the monitoring of the reaction rate in the CSTR, $r = Qy_{CO_2}$, where Q, the net flowrate, was maintained at 170 μmol/s at all times. In most cases, the time necessary for the rate to reach the steady-state value was of the order of a few minutes. At 550°C, some 24 h were allowed between successive experiments for the emf to reach a constant value (± 2 mV). At 500°C, the period necessary to obtain a stable emf (± 5 mV) was about 48 h.

Two similar oxide electrodes were investigated. Before the steady-state experiments the A-La(Sr)MnO_3 electrode (S_A = 98 cm^2) had been subjected to preliminary successive reduction–reoxidation experiments at 500°C over a period of three months. Conversely, the B-La(Sr)MnO_3 electrode (S_B = 232 cm^2) was used after an initial deactivation period (one week on 15.5% O_2, 6% CO stream).

In Fig. 2, the rate and emf measurements obtained on the A-La(Sr)MnO_3 electrode at 550°C and 6% CO are plotted against the gas phase O_2 concentration. The experiments were done at sequentially decreasing followed by sequentially increasing O_2 concentrations in the range 2–16%. Two successive cycles were performed. A very pronounced hysteresis effect is observed during the first cycle. The rate of reaction is determined not only by the gas phase composition but also by the catalyst oxygen activity. The steep increase in the rate near the stoichiometric point $CO/O_2 = 2$ is accompanied by a steep decrease in the emf. During the second cycle, the hysteresis in the rate and the emf is less pronounced. It can be seen that in all cases, at constant gas phase compositions, lower oxygen activity values correspond to higher rate values.

The "error bar" in Fig. 2 presents the error in the measurement of the rate, i.e., 2×10^{-2} μmol/s, associated with the accuracy of the IR spectrometer. It will be omitted in the following graphs (550°C) for clarity. The repeatability of the measurements can be estimated by the three points at 15.5% O_2 ($r = 34 \pm 2 \times 10^{-2}$ μmol/s) which correspond to the same emf value (= −70 mV); this indicates an error of 5% in the rate.

In Fig. 3, the rate and emf measurements obtained on the A-electrode at sequentially increasing followed by sequentially decreasing CO concentrations at 550°C and 5% O_2 are plotted against the percentage of CO. The hysteresis is not as pronounced as in the oxygen cycle. Furthermore, the opposite pattern appears; at constant gas phase composition, the rate increases when the oxygen activity increases.

Cycles of O_2 and CO were carried out over the B-electrode, at 550°C. The results at 6% CO are plotted in Fig. 4. Again, the rate and the emf exhibit simultaneously multiple steady states. No steep rate increase appears around the stoichiometric point. At constant gas phase composition, the rate decreases when the emf increases. This observation is also true during the CO cycles at 5% O_2 (Fig. 5), in contrast to the A-electrode.

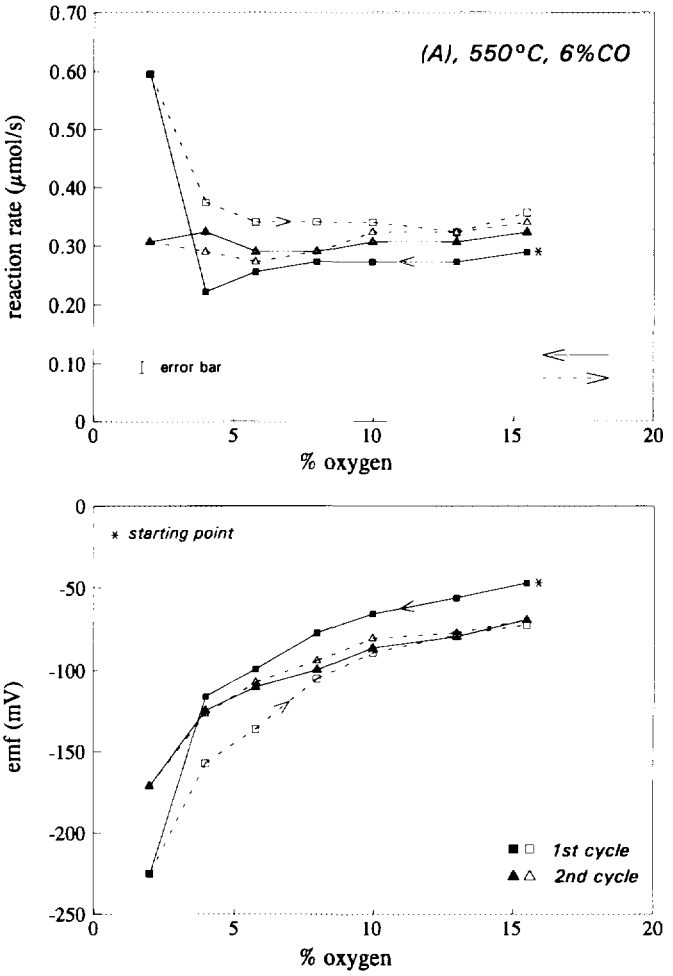

FIG. 2. Steady-state rate and emf measurements during CO oxidation at 550°C and 6% CO on A-La(Sr)MnO_3 catalyst. Closed (open) symbols signify the measurements at decreasing (increasing) percentages of O_2. Squares (triangles) denote the data during the first (second) cycle.

In Fig. 6, the rate and emf measurements obtained on the A-La(Sr)MnO_3 electrode at 500°C and 6% CO are plotted against the gas phase O_2 concentration. The emf shows significant hysteresis, indicating that the oxygen activity of the La(Sr)$MnO_{3-\delta}$ catalyst can change substantially at constant compositions of the gas phase. The rate of reaction seems to be relatively insensitive to such variations (compare the error bars in Figs. 2 and 6). The rate appears to depend only on the gas phase composition and not on the catalyst oxygen activity. There does, however,

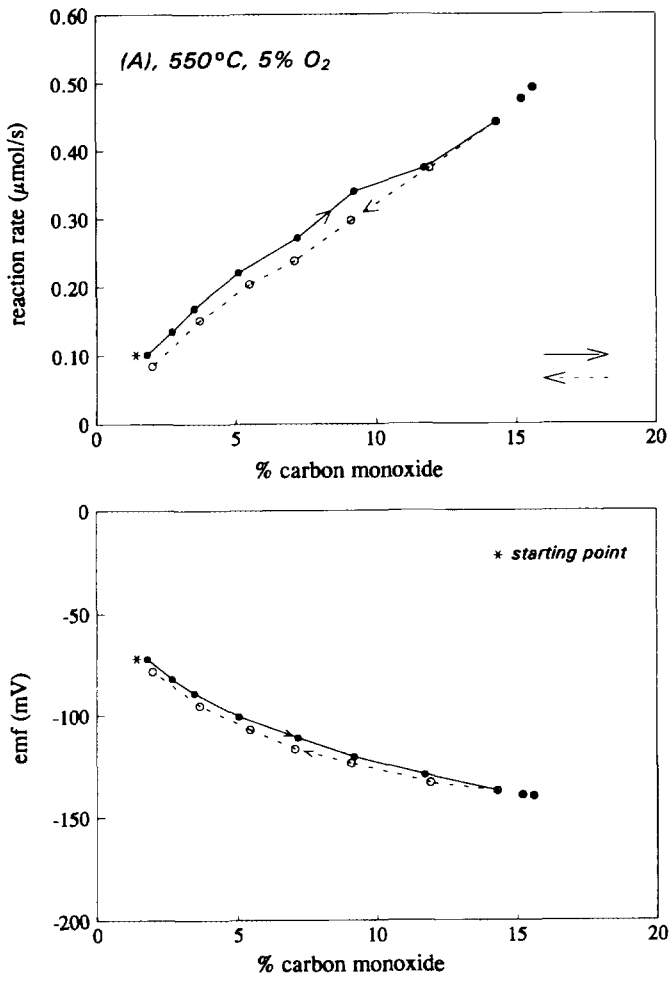

FIG. 3. Steady-state rate and emf measurements during CO oxidation at 550°C and 5% O_2 on A-La(Sr)MnO_3 catalyst. Closed (open) symbols signify the measurements at increasing (decreasing) percentages of CO.

appear to be a systematic difference in the rate at decreasing P_{O_2} versus increasing P_{O_2}; the reason for this will be discussed later.

In Fig. 7, experimental data on the B-electrode at 500°C are presented. During the CO-cycle at 5% O_2, the emf shows hysteresis, while the rate does not. Again, the rate of reaction appears to be independent of the oxygen activity of the catalyst.

CO-cycles on the A-electrode and O_2-cycles on the B-electrode were also performed at 500°C. For clarity, the data are not presented here.

DISCUSSION

The Charge Transfer Reaction

The chemical and electrochemical reactions at the mixed conducting p-type La(Sr)$MnO_{3-\delta}$/YSZ electrode can be written, in general terms (11, 21), as adsorption of oxygen

$$O_2(g) + 2S \rightleftarrows 2OS, \qquad [2]$$

surface diffusion to the three-phase gas/oxide/YSZ boundary (tpb) line

$$OS + S_{(tpb)} \rightleftarrows S + OS_{(tpb)}, \qquad [3]$$

charge transfer reaction at the tpb

$$OS_{(tpb)} + V^{\cdot\cdot}_{O(YSZ)} \rightleftarrows S_{(tpb)} + O^{x}_{O(YSZ)} + 2h^{\cdot}, \qquad [4]$$

incorporation of oxygen into the lattice

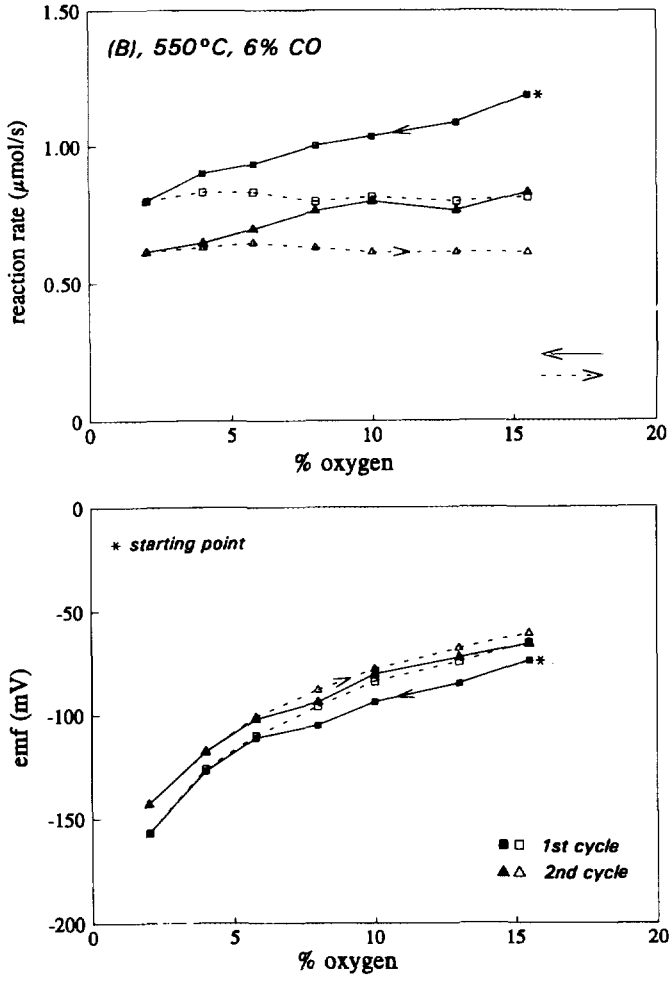

FIG. 4. Steady-state rate and emf measurements during CO oxidation at 550°C and 6% CO on B-La(Sr)MnO_3 catalyst. Closed (open) symbols signify the measurements at decreasing (increasing) percentages of O_2. Squares (triangles) denote the data during the first (second) cycle.

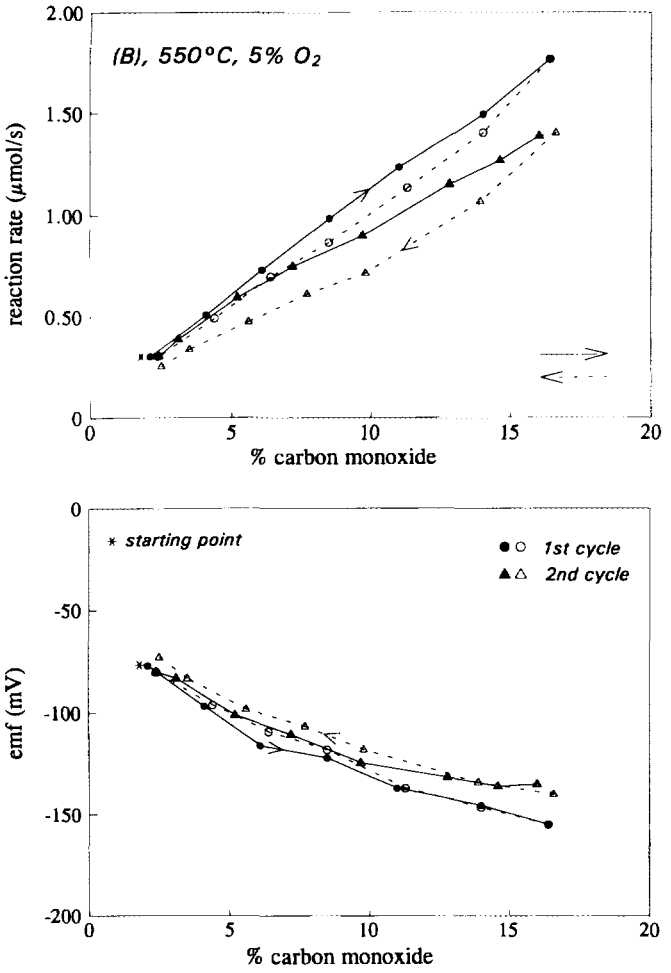

FIG. 5. Steady-state rate and emf measurements during CO oxidation at 550°C and 5% O_2 on B-La(Sr)MnO_3 catalyst. Closed (open) symbols signify the measurements at increasing (decreasing) percentages of CO. Circles (triangles) denote the data during the first (second) cycle.

$$OS + V^{\cdot\cdot}_{O(s)} + 2Mn^{x}_{Mn} \rightleftarrows S + O^{x}_{O(s)} + 2Mn^{\cdot}_{Mn}, \quad [5]$$

lattice diffusion to the bulk

$$O^{x}_{O(s)} + V^{\cdot\cdot}_{O(b)} \rightleftarrows V^{\cdot\cdot}_{O(s)} + O^{x}_{O(b)}, \quad [6]$$

lattice diffusion to the oxide/YSZ interface

$$O^{x}_{O(b)} + V^{\cdot\cdot}_{O(int)} \rightleftarrows V^{\cdot\cdot}_{O(b)} + O^{x}_{O(int)}, \quad [7]$$

charge transfer reaction at the two-phase oxide/YSZ interface

$$O^{x}_{O(int)} + 2Mn^{\cdot}_{Mn} + V^{\cdot\cdot}_{O(YSZ)} \rightleftarrows V^{\cdot\cdot}_{O(int)} + 2Mn^{x}_{Mn} + O^{x}_{O(YSZ)} + 2h^{\cdot}, \quad [8]$$

where, according to Kröger–Vink notation, O^{x}_{O} is a lattice oxygen atom, $V^{\cdot\cdot}_{O}$ is a double positively charged oxygen vacancy, and Mn^{x}_{Mn}, $Mn^{\cdot}_{Mn}$ are manganese ions in the 3+ and 4+ state, respectively.

Hammouche *et al.* (21) examined the kinetics of oxygen reduction at the YSZ/$La_{1-x}Sr_xMnO_3$ (x = 0–0.5) electrode in air at 960°C, by means of steady-state and transient polarization measurements. At low cathodic polarization the charge transfer reaction occurred at the triple points [4] and the electrode behaviour was similar to that of metals. At high cathodic polarization, oxide vacancies were created and the rate was increased due to the broadening of the effective electrode reaction zone; the electrochemical reaction would then involve the diffusion of oxygen into the lattice and the charge transfer at the two-phase interface [8]. The latter reaction was limited by the diffusion step [6], [7].

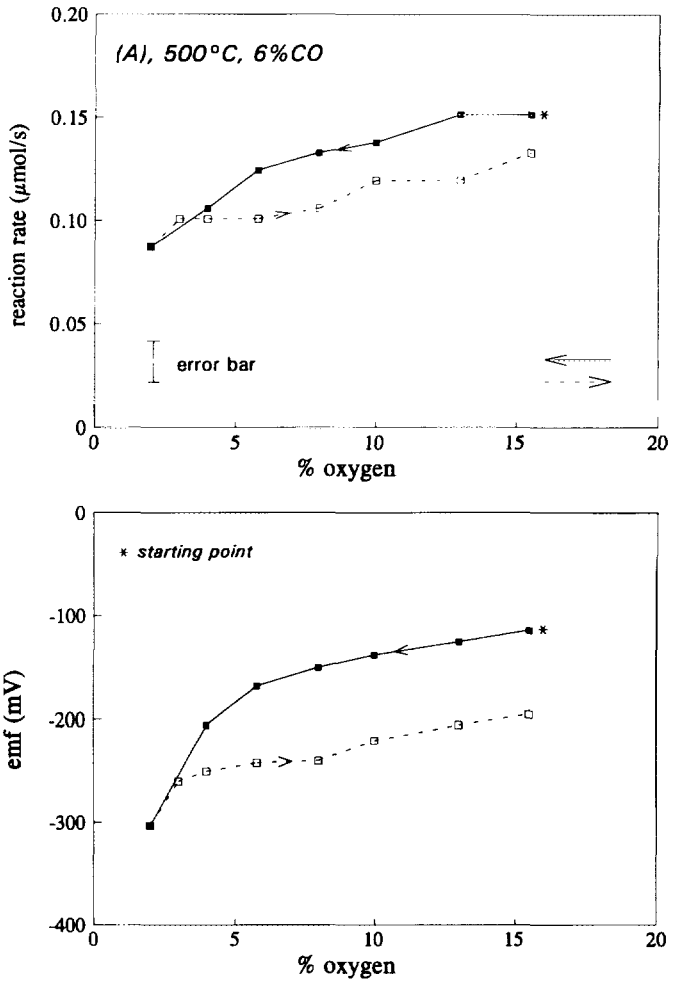

FIG. 6. Steady-state rate and emf measurements during CO oxidation at 500°C and 6% CO on A-La(Sr)MnO_3 catalyst. Closed (open) symbols signify the measurements at decreasing (increasing) percentages of O_2.

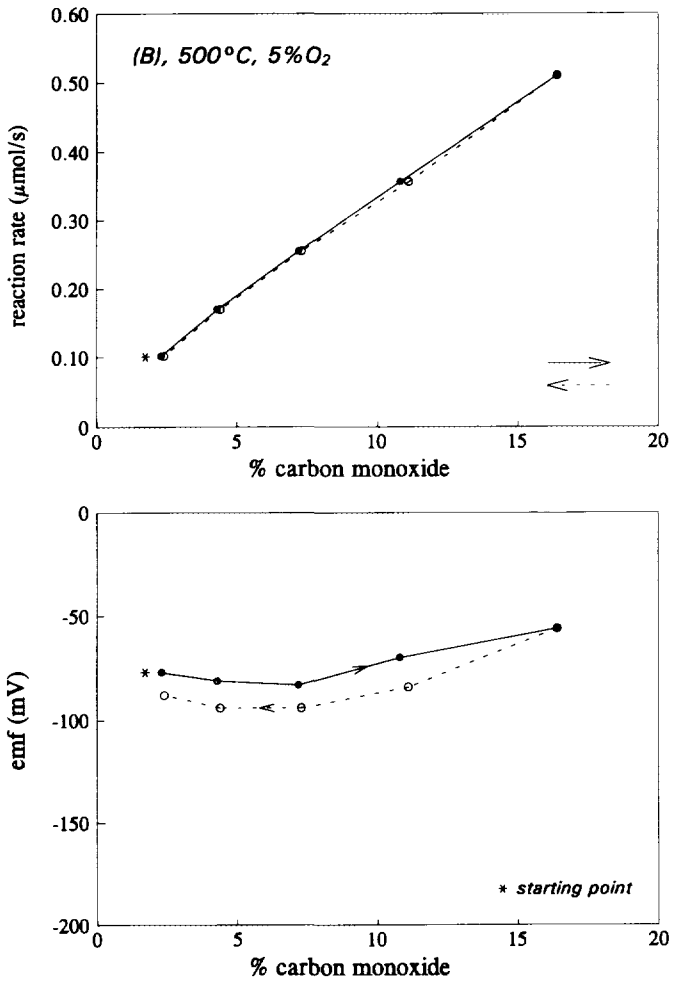

FIG. 7. Steady-state rate and emf measurements during CO oxidation at 500°C and 5% O_2 on A-La(Sr)MnO_3 catalyst. Closed (open) symbols signify the measurements at decreasing (increasing) percentages of CO.

The three-phase and two-phase charge transfer reactions as indicated in [4] and [8], respectively, can be generally considered as two possible pathways of the same electrocatalytic reaction rather than two different competing reactions. The discrimination between them suggested by Hammouche *et al.* (21) is a question of kinetics. The reaction at the "triple points," is a charge transfer limited reaction since the surface diffusion [3] of the oxygen species is fast. The overall two-phase charge transfer reaction [6]–[8] involves the diffusion of oxygen ions through the oxide lattice. If lattice diffusion were fast, then the two-phase reaction would be kinetically similar to a tpb reaction.

For the emf generation (SEP), the discrimination between the three- and the two-phase reactions can be made in terms of the oxygen species that participate in each one. This is important when examining the relationship between the rate of reaction and the SEP oxygen activity. The rate of reaction will depend on the concentrations of the active surface species. These species could be adsorbed oxygen or surface lattice oxygen. The emf will measure the activity of those species that participate in the charge transfer reaction. If this proceeds at the "triple points" utilizing surface oxygen, the emf may measure the activity of the oxygen species which participate in the chemical reaction. On the other hand, if the charge transfer reaction involves bulk oxygen then the emf may only reflect the oxidation state of the catalyst.

One can argue that charge transfer in oxide electrodes can occur not only in the tpb region, broadened or not, but everywhere across the oxide/YSZ interface; i.e., oxygen atoms from the oxide bulk can be transferred to the electrolyte according to Eq. [8]. At steady state, these species will be in equilibrium with the lattice oxygen in the broadened tpb in order to have a uniform potential in the interface, but not necessarily in equilibrium with the oxygen species of the catalyst surface. This suggests that the SEP oxygen activity may be a bulk quantity. It would reflect the activity of the oxygen in the oxide lattice; it would also reflect the active surface species if equilibrium were established between the oxide bulk and the surface. However, one may consider a situation where the oxygen transfer between the oxide bulk and the YSZ has not yet reached equilibrium. This may happen when the ionic conductivity of the oxide is much lower than its electronic conductivity. In this case, one can consider two-charge transfer reactions taking place; the one at the tpb will be in equilibrium, while the other one at the two-phase boundary will not. The emf will then reflect the catalyst surface and not the bulk.

In the previous SEP studies on oxide catalysts (4–6), it has been assumed that the measured oxygen activity is a bulk quantity. This argument was supported by the fact that the time necessary for the emf to approach a stationary value was an order of magnitude higher than the time needed for the rate to reach steady state (5). This was also observed in this work between the successive experiments in O_2 or CO cycles and during transients (19). When a reacting mixture (6% CO, 15.5% O_2) was imposed on a preoxidized catalyst at 500°C, the rate achieved the steady-state value within minutes, while more than 72 h was required for the emf to reach a stationary state. Taking into account that porous electrode films are employed, as indicated by the SEM, one can suggest that oxygen-ion diffusion is taking place. The time necessary for the oxide lattice to reconstruct is more than that for the surface to do so. This was also seen when an O_2/N_2 mixture replaced a reacting mixture (6% CO, 15.5% O_2). The rate of reaction went to zero within 4–5 min, while the emf value (−50 and −60 mV) was still close to its original value (−72 mV) and far from its steady-state value of

+5 mV. The charge transfer reaction at the two-phase interface [8] seems to operate even in O_2/inert gas atmospheres, indicating the importance of the ionic conductivity of the oxide.

Following the above considerations, it seems reasonable to assume that the SEP oxygen activity of the La(Sr)MnO_3 catalyst in the experimental conditions employed is a measure of the bulk oxygen species, the oxidation state of the catalyst. The equilibrium potential difference across the oxide/YSZ interface $\Delta\phi_e$, can be obtained by equating the rates of the cathodic and anodic reactions in Eq. [8],

$$\Delta\phi_e = \frac{RT}{2F}\ln\left(\frac{k_c'[O^x_{O(int)}][Mn^{\cdot}_{Mn}]^2}{k_a'[V^{\cdot\cdot}_{O(int)}][Mn^x_{Mn}]^2}\right), \qquad [9]$$

where $k_c' = k_c[V^{\cdot\cdot}_{O(YSZ)}]$ and $k_a' = k_a[O^x_{O(YSZ)}]$ are modified cathodic and anodic charge transfer coefficients.

The potentiometric oxygen activity will be given by means of the Nernst equation

$$\alpha_O = P^{1/2}_{O_2,R}\exp\left(\frac{2F}{RT}E\right) = \frac{1}{K}\exp\left(\frac{2F}{RT}\Delta\phi_e\right). \qquad [10]$$

K is the equilibrium constant of the overall electrochemical reduction of oxygen, $K = K_2^{1/2}K_5K_6K_7K_8$, where K_2, K_5, K_6, K_7, and $K_8 = k_c/k_a$ are the equilibrium constants of the reactions [2], [5], [6], [7], and [8].

Assuming that oxygen at the oxide/YSZ interface is in equilibrium with bulk oxygen (Eq. [7]), the oxygen activity will be

$$K_b\alpha_O = \frac{[O^x_{O(b)}][Mn^{\cdot}_{Mn}]^2}{[V^{\cdot\cdot}_{O(b)}][Mn^x_{Mn}]^2} = \frac{[O_b]}{[V_b]}, \qquad [11]$$

where $K_b = KK_7^{-1}K_8^{-1} = K_2^{1/2}K_5K_6$ stands for the equilibrium constant of the combined reaction

$$\tfrac{1}{2}O_2(g) + V^{\cdot\cdot}_{O(b)} + 2Mn^x_{Mn} = O^x_{O(b)} + 2Mn^{\cdot}_{Mn}, \qquad [12]$$

which describes the incorporation (absorption) of oxygen into the oxide lattice. For convenience, $[O_b]$ is defined to equal $[O^x_{O(b)}][Mn^{\cdot}_{Mn}]^2$ and $[V_b] = [V^{\cdot\cdot}_{O(b)}][Mn^x_{Mn}]^2$.

If equilibrium is established between the bulk and the surface species [5], [6] then the SEP oxygen activity will reflect the oxygen species that participate in the chemical reaction

$$K_O\alpha_O = \frac{\theta_{OS}}{\theta_S}, \qquad [13]$$

where $K_O = KK_5^{-1}K_6^{-1}K_7^{-1}K_8^{-1} = K_2^{1/2}$ is the oxygen adsorption equilibrium constant. If, furthermore, reaction [2] is in equilibrium then $\alpha_O = P^{1/2}_{O_2}$.

The oxygen activity is not measuring a concentration, i.e., the oxygen nonstoichiometry of La(Sr)$MnO_{3-\delta}$, but a virtual oxygen pressure (1, 2) in equilibrium with the oxide lattice (12). The relationship between the oxygen nonstoichiometry, δ, of the catalyst and the oxygen activity can be examined by means of thermogravimetric measurements. The emf values observed under reaction conditions in this work were in the range of -45 to -300 mV. Using the TGA data of Mizusaki *et al.* (22), one can estimate that these values correspond to a nonstoichiometry of $3 - \delta \approx 3$ and $3 - \delta \approx 2.98$, respectively (19). This suggests that phase transformations of the perovskite catalyst do not occur under reaction conditions.

It may be possible at low voltages for the electrochemical reaction of CO with the oxygen ions of the electrolyte to occur,

$$CO(g) + O^x_{O(YSZ)} \rightarrow CO_2(g) + V^{\cdot\cdot}_{O(YSZ)} + 2e', \qquad [14]$$

and a "mixed potential" will then be measured (17). Summarizing SEP studies on metals, Vayenas *et al.* (3) suggested that when emf values higher than -400 mV are observed, one can assume that no "mixed potential" is present. For oxide electrodes one can furthermore postulate that, because oxygen ions in the electrode surface are easily available, CO may preferentially react with them rather than with O^{2-} of the electrolyte. Nevertheless, the emf values measured in this work were always higher than -300 mV. One can then assume that no charge transfer reactions other than the reversible reduction of oxygen were taking place and the oxygen activity can be determined by means of the Nernst equation [10].

The Ionic Redox Model

The *ionic*[2] redox model (23–25) assumes that the reduction and reoxidation reactions are taking place at different sites on the catalyst surface. Oxygen ions are then transported through the oxide lattice from the sites *ox*, where incorporation of gas phase oxygen takes place, to the sites *r*, where they react with CO. The reaction mechanism will then include the following steps:

—reoxidation of the ox-sites by gas phase oxygen (the adsorption of oxygen)

$$O_2(g) + S_{ox} \rightarrow O_2S_{ox} \qquad [15]$$

$$O_2S_{ox} + S_{ox} \rightleftharpoons 2OS_{ox}; \qquad [16]$$

[2] The term *ionic* redox model is first proposed here.

—diffusion of oxygen species from the ox-sites to the bulk (reoxidation of the bulk)

$$OS_{ox} + V_b = S_{ox} + O_b; \quad [17]$$

—diffusion of oxygen species from the bulk to the r-sites (reoxidation of the r-sites)

$$O_b + S_r = V_b + OS_r; \quad [18]$$

—reduction reaction of oxygen with CO at the r-sites

$$CO(g) + OS_r \rightarrow CO_2(g) + S_r. \quad [19]$$

The scheme can be considered to consist of two overall reactions, namely the processes of the reoxidation and the reduction of the solid catalyst which contain the steps [15]–[17] and [18], [19], respectively.

Similar dual-site redox models have often been proposed in the literature (24, 25) to describe the mechanism of the selective oxidation of propene to acrolein on mixed oxides, e.g., Bi_2O_3–MoO_3. It is usually assumed that, due to the high mobility of oxygen species in these oxides, the lattice diffusion is infinitely fast compared to the surface reactions [26]. Accordingly the processes [17] and [18] are in equilibrium, i.e.,

$$K_{ox} = \frac{[O_b](1 - \theta_{ox})}{[V_b]\theta_{ox}}, \quad K_r = \frac{[O_b](1 - \theta_r)}{[V_b]\theta_r}, \quad [20]$$

where θ_{ox} and θ_r stand for the coverages of oxygen species at the ox- and r-sites, respectively. Thermodynamically, the two sites are similar,

$$K_{ox} = K_r. \quad [21]$$

The SEP oxygen activity is given by Eq. [11],

$$K_b\alpha_O = \frac{[O_b]}{[V_b]}, \quad [22]$$

where K_b is the "absorption" equilibrium constant describing the incorporation of oxygen into the oxide lattice. The oxygen adsorption equilibrium constant, K_O, will be

$$K_O = K_b/K_{ox} = K_b/K_r. \quad [23]$$

Accordingly,

$$\theta_{ox} = \frac{K_O\alpha_O}{1 + K_O\alpha_O}, \quad \theta_r = \frac{K_O\alpha_O}{1 + K_O\alpha_O}. \quad [24]$$

The concentration of oxygen at the r-sites will then be equal to the concentration of oxygen at the ox-sites.

The rates of the reoxidation and reduction reactions will be given by

$$r_{ox} = k_{ox}P_{O_2}(1 - \theta_{ox}) = \frac{k_{ox}P_{O_2}}{1 + K_O\alpha_O} \quad [25]$$

$$r_r = k_rP_{CO}\theta_r = \frac{k_rP_{CO}K_O\alpha_O}{1 + K_O\alpha_O}. \quad [26]$$

At steady state,

$$\frac{d[O_b]}{dt} = \frac{k_{ox}P_{O_2}}{1 + K_O\alpha_O} - \frac{k_rP_{CO}K_O\alpha_O}{1 + K_O\alpha_O} = 0 \quad [27]$$

and the oxygen activity and the rate of reaction will be

$$\alpha_O = \frac{k_{ox}}{K_Ok_r}\frac{P_{O_2}}{P_{CO}} \quad [28]$$

$$r = \frac{k_{ox}k_rP_{O_2}P_{CO}}{k_{ox}P_{O_2} + k_rP_{CO}}. \quad [29]$$

The kinetic expression [29] of the ionic redox model is then similar to the kinetic expression that would be obtained by a Mars–van Krevelen redox model (27) where the reoxidation of the reduced sites occurs by the gas phase oxygen (single-site mechanism). This is the result of the assumption that the lattice diffusion of oxygen is fast and the exchange of oxygen between the ox- and the r-sites is in equilibrium. Equations [28] and [29], which express the relationships between the oxygen activity/reaction rate and the gas phase composition, will be referred to hereafter as Mars–van Krevelen equations.

Steady-state multiplicity as well as reaction rate oscillations in catalytic oxidations have often been attributed to phase transformations of the solid catalyst (28, 29). The different phases of the catalyst exhibit different kinetic coefficients (or even rate laws). The thermodynamic stability limits of a certain phase are designated by a region of the oxygen activity; the rate constants are then some stepwise functions of the catalyst oxygen activity. Transitions between the nonequilibrium phases will cause hysteresis or oscillatory patterns in the oxygen activity and accordingly in the rate of reaction. This has been demonstrated by means of SEP in systems such as Pt/PtO_x (30–32), Ni/NiO (33), and $Cu_2O/CuO/Cu$ (4, 34).

The stability of the perovskite structure La(Sr)$MnO_{3-\delta}$ in the experimental conditions employed indicates that different phases of the oxide catalyst (e.g., the simple oxides) were not formed. Accordingly, for given values of

the reduction and reoxidation coefficients, the Mars–van Krevelen equations suggest that the rate and the oxygen activity are determined solely by the gas phase composition and multiple steady states would not be observed. This is because equilibrium between oxygen species in the bulk and the surface has been assumed. The assumption, however, of the fast ionic diffusion may not be valid in solids where only a small fraction of the lattice oxygen is involved in the reaction (26). This may be the case for the La(Sr)$MnO_{3-\delta}$ catalyst, where the variation of δ is small in the range of the experimental conditions employed. Diffusional limitations may then appear during (a) the reoxidation of the reduction sites or (b) the reoxidation of the bulk.

(*a*) *Reoxidation determined reaction.* The reoxidation of the r-sites is not infinitely fast compared to the reaction with CO; i.e., the r-oxygen species is not in equilibrium with the bulk oxygen [18]. Conversely, the exchange of oxygen between the ox-sites and the bulk [17] remains in equilibrium; i.e., the reoxidation of the bulk is infinitely fast compared to the oxygen adsorption. The rates of the reoxidation and reduction reactions will be given by

$$r_{ox} = k_{ox}P_{O_2}(1 - \theta_{ox}) = \frac{k_{ox}P_{O_2}}{1 + K_O\alpha_O} \qquad [25]$$

$$r_r = k_rP_{CO}\theta_r \neq \frac{k_rP_{CO}K_O\alpha_O}{1 + K_O\alpha_O}. \qquad [26a]$$

The diffusion of oxygen species to the r-sites should proceed through hopping of oxygen atoms from the bulk, O_b, to neighbouring vacancies $V_{n-1}, \ldots, V_i, \ldots, V_2$, on the way to the surface sites, S_r,

$$O_b + V_{n-1} \rightarrow V_b + O_{n-1} \qquad [18a]$$

$$O_i + V_{i-1} \rightarrow V_i + O_{i-1} \qquad [18b]$$

$$O_{2,r} + S_r \rightarrow V_{2,r} + OS_r, \qquad [18c]$$

where the subscripts denote the oxide layers below the surface; V_{n-1} is a vacancy deep in the oxide and V_2 a vacancy adjacent to the surface. At steady state, the rate of the reoxidation equals the rate of the diffusion process, f,

$$\frac{d[O_b]}{dt} = \frac{k_{ox}P_{O_2}}{1 + K_O\alpha_O} - f([O_{i-1}][V_i]) = 0, \qquad [27a]$$

where f is a function of the concentrations of lattice oxygen species and oxygen vacancies. Equation [27a] is nonlinear; the oxygen activity can exhibit different values at a certain composition of the gas phase. An increase, for example, in the concentration of the oxide vacancies will increase the coverage of the vacant ox-sites [17] and accordingly the rate of oxygen adsorption [25]. The increase in the number of lattice oxygen vacancies will also increase the rate of the oxygen diffusion [18a]–[18c].

The solid catalyst will in general exhibit multiple oxygen activity values and accordingly multiple steady-state rates at constant gas phase compositions. The rate of reaction will be given by "reoxidation kinetics" as a function of the oxygen partial pressure and the catalyst oxygen activity. A *reoxidation determined reaction* is then said to be taking place, as a simple kinetic expression based on the catalyst reoxidation reaction can be employed.

(*b*) *Reduction determined reaction.* The reoxidation of the bulk is not infinitely fast compared to the oxygen adsorption, i.e., the ox-sites are not in equilibrium with bulk vacancies. The exchange of oxygen between the r-sites and the bulk [4] is assumed to be in equilibrium; i.e., the reoxidation of the r-sites is infinitely fast compared to the reaction with CO. The rates of the reoxidation and reduction reactions will then be

$$r_{ox} = k_{ox}P_{O_2}(1 - \theta_{ox}) \neq \frac{k_{ox}P_{O_2}}{1 + K_O\alpha_O} \qquad [25b]$$

$$r_r = k_rP_{CO}\theta_r = \frac{k_rP_{CO}K_O\alpha_O}{1 + K_O\alpha_O}. \qquad [26]$$

The reaction rate can be determined by "reduction kinetics" as a function of the partial pressure of carbon monoxide and the catalyst oxygen activity. A *reduction determined reaction* is then said to be taking place. The reaction kinetics suggest that in a certain gas phase mixture the rate increases when the oxygen activity increases. This is due to an increase in the concentration of r-oxygen species [18] and accordingly in the rate of the CO reaction [19].

In the above analysis it was assumed that the rates of the overall reduction and reoxidation of the solid catalyst are determined by the corresponding surface reactions, i.e., the reaction with CO and the adsorption of oxygen, respectively, and not by the diffusion processes. This is in agreement with the general idea of a redox scheme consisting of two irreversible steps separated in time (Mars–van Krevelen) and/or in space (ionic redox model). The ionic redox model will be employed in the next section to describe the results at 550°C.

One may suggest that a third situation may be possible where both the ox- and the r-sites are not in equilibrium with the bulk; the rate of reaction could not then be determined by means of the oxygen activity. However, if the overall diffusion of oxygen to the oxide lattice was limited, then one may expect other mechanisms to become domi-

nant. The reaction might then proceed by reoxidation of the reduced sites with gas phase oxygen. This will be demonstrated during the interpretation of the results at 500°C.

The Multiple Steady States (550°C)

The rate of reaction exhibits multiple steady states at a certain gas phase composition at 550°C. Multiplicity appears, at the same time, in the oxygen activity of the catalyst. This suggests that the rate is a function not only of the gas phase composition but also of the oxygen activity.

The experimental data on B-La(Sr)MnO_3 indicate that a one-to-one correlation exists between the rate and the emf. At constant gas phase compositions, the rate always increases when the oxygen activity decreases. This suggests that, according to the ionic redox model, a *reoxidation determined* reaction is taking place. The data are satisfactorily fitted to reoxidation kinetics (linearized form)

$$\frac{P_{O_2}}{r} = \frac{1}{k_{ox}} + \frac{K_O}{k_{ox}}\alpha_O \qquad [30]$$

(B) $k_{ox} = 51.8\ \mu\text{mol s}^{-1}\text{ bar}^{-1}$, $K_O = 244\ \text{bar}^{-1/2}$.

In Fig. 8a a plot of P_{O_2}/r against α_O is presented. Squares and circles indicate the data obtained during the O_2- and CO-cycles, respectively. Predicted values are shown by the solid line. A discrepancy appears only for the starting point at 15.5% O_2 of the first oxygen cycle at 6% CO. Conversely, the reduction kinetics (linearized form)

$$\text{(B)}\quad \frac{P_{CO}}{r} \neq \frac{1}{k_r} + \frac{1}{k_r K_O}\frac{1}{\alpha_O} \qquad [31]$$

fails to predict the data; the plot of P_{CO}/r vs $1/\alpha_O$ is presented in Fig. 8b.

The data on A-La(Sr)MnO_3 suggest that the relationship between the rate and the emf is not straightforward. In most cases, the rate increases when the oxygen activity decreases, at constant gas phase compositions, e.g., the 3-fold increase of the rate at 2% O_2 during the first O_2-cycle (Fig. 2). However, in other cases, the rate was found to decrease upon decreasing oxygen activity (Fig. 3). In Fig. 9a a plot of P_{O_2}/r vs α_O is presented. Squares and triangles denote measurements during the first and second O_2-cycles, respectively; circles indicate the measurements during the CO-cycle. The reoxidation kinetics

$$\frac{P_{O_2}}{r} = \frac{1}{k_{ox}} + \frac{K_O}{k_{ox}}\alpha_O \qquad [32]$$

(A) $k_{ox} = 18.2\ \mu\text{mol s}^{-1}\text{ bar}^{-1}$, $K_O = 225\ \text{bar}^{-1/2}$

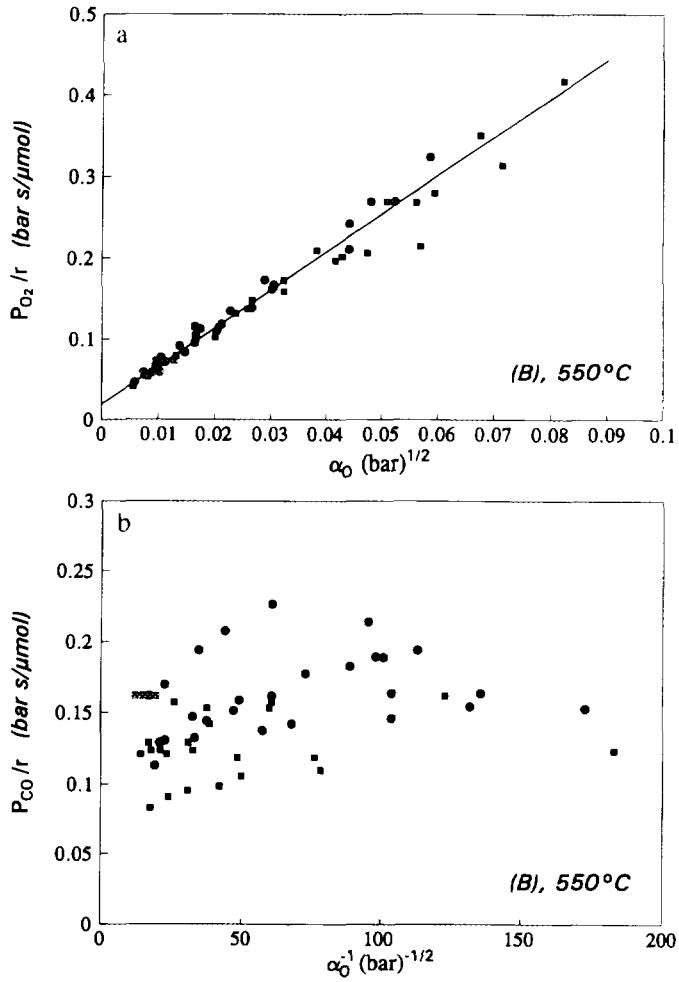

FIG. 8. Reoxidation (a) and reduction (b) kinetics at 550°C on B-La(Sr)MnO_3 catalyst. Squares and circles signify the measurements during the O_2- (Fig. 4) and CO-cycles (Fig. 5), respectively.

predicts satisfactorily the majority of the experimental data. Significant deviations occur for the data obtained at 6% CO (first cycle) at successively decreasing P_{O_2}. A systematic deviation also exists for the data at 5% O_2 at successively decreasing P_{CO}. In Fig. 9b a plot of r/P_{CO} vs α_O is shown (the scale of the linearized form is inappropriate). A good agreement exists between those experimental data that were not described by [32] and the predictions of the reduction kinetics,

$$\frac{r}{P_{CO}} = \frac{k_r K_O \alpha_O}{1 + K_O \alpha_O} \qquad [33]$$

(A) $k_r = 2.99\ \mu\text{mol s}^{-1}\text{ bar}^{-1}$, $K_O = 173\ \text{bar}^{-1/2}$.

A distinct separation of the data points into two groups is suggested. These correspond to the *reoxidation determined* and *reduction determined* reaction regimes, pre-

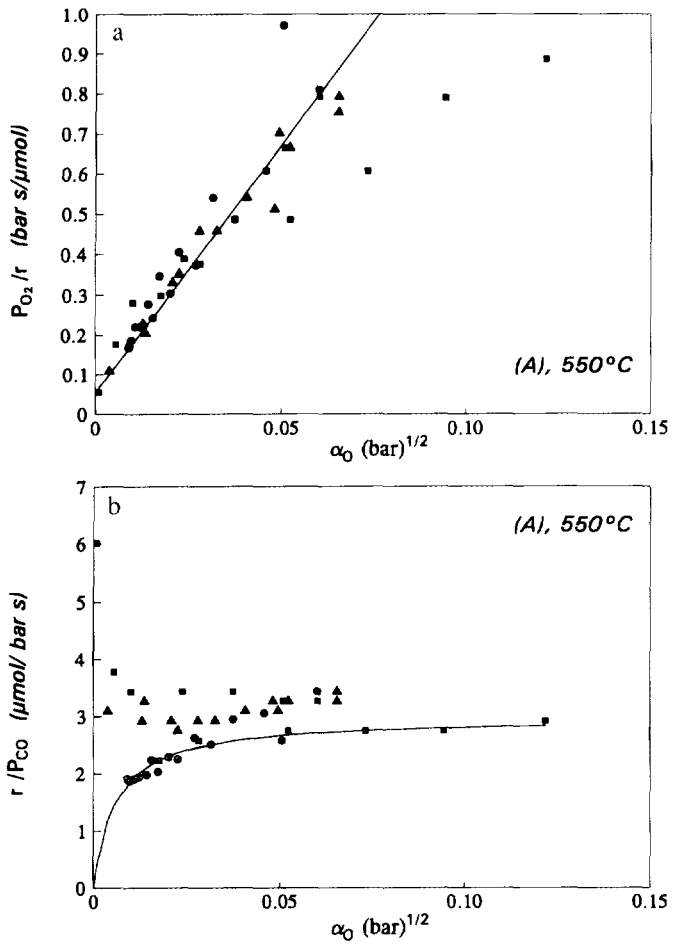

FIG. 9. Reoxidation (a) and reduction (b) kinetics on A-La(Sr)MnO_3 catalyst at 550°C. Squares, triangles, and circles signify the data during the first O_2-cycle (Fig. 2), the second O_2-cycle (Fig. 2), and the CO-cycle (Fig. 3), respectively.

dicted by the ionic redox model. The kinetic expressions [32] and [33] estimate similar values for the equilibrium constant, K_O, confirming the validity of Eqs. [21] and [23]. Note that the reaction changed from reduction to reoxidation determined at the stoichiometric point during the first oxygen cycle (Fig. 2), causing the steep increase in the rate and the similar decrease in the oxygen activity.

The behaviour of the A-La(Sr)MnO_3 catalyst can be demonstrated by the plot of "*the error of reoxidation kinetics.*" In Fig. 10a the ratio of the experimental rate over the rate predicted by reoxidation kinetics [32], r_{exp}/r_{ox}, is plotted against $(P_{CO}/P_{O_2})\alpha_O$, a term which expresses the ratio of reduction over reoxidation kinetics,

$$\frac{r_r}{r_{ox}} = \frac{k_r K_O}{k_{ox}} \frac{P_{CO}\alpha_O}{P_{O_2}}. \qquad [34]$$

The r_{exp}/r_{ox} values will be scattered around unity if the reaction is reoxidation determined. Conversely, when the reaction follows reduction kinetics, then the data should be described by a straight line passing through the origin of the axis.

$$\frac{r_{exp}}{r_{ox}} = \begin{cases} 1, & r_{exp} = r_{ox} \\ \dfrac{k_r K_O}{k_{ox}} \dfrac{P_{CO}\alpha_O}{P_{O_2}}, & r_{exp} = r_r. \end{cases} \qquad [35]$$

In Fig. 10a the two groups of experimental points on A-La(Sr)MnO_3 that correspond to the reoxidation and reduction determined reaction regimes are shown. Given the k_{ox} and K from Eq. [32], the reduction coefficient k_r can be estimated from the gradient of the solid line to be 2.90 μmol s^{-1} bar^{-1}, in good agreement with the fit in Eq. [33]. The point where the reduction and reoxidation curves cross

$$\frac{\alpha_O^* P_{CO}}{P_{O_2}} \approx \frac{k_{ox}}{K_O k_r} \qquad [36]$$

signifies the oxygen activity value, α_O^*, predicted by the Mars–van Krevelen equation [28], that corresponds to the equilibrium between the ox- and the r-sites (fast ionic diffusion). The plot also allows a comparison between experimental error, appearing for example at low $(P_{CO}/P_{O_2})\alpha_O$ values (probably because the final steady state had not been achieved), and "systematic" error, associated with a transition to a reduction determined reaction.

In Fig. 10b the plot of the "error of reoxidation kinetics" for B-La(Sr)MnO_3 is presented. An agreement in the range of 10% exists between the experimental data and the predictions of the model. "Systematic" error does not appear in this case. The reaction on B-La(Sr)MnO_3 is always reoxidation determined, in contrast with the behaviour of A-La(Sr)MnO_3, where transitions in the reaction regime are taking place. (It should be noted that a reduction determined reaction regime was observed on B-La(Sr)MnO_3 during other experiments.)

The values of the adsorption equilibrium constant, K_O, were found to be 225 and 244 $bar^{-1/2}$ for the A- and B-La(Sr)MnO_3 electrodes, respectively. This similarity indicates the fact that K_O is an oxide-specific constant, for a given temperature. Conversely, the kinetic coefficients of the two electrodes were remarkably different. The reoxidation coefficient, k_{ox}, of B-La(Sr)MnO_3 is 2.8 times higher than the reoxidation coefficient of A-La(Sr)MnO_3, $k_{ox,B}/k_{ox,A}$ = 51.8/18.2 = 2.8. This is in good agreement with the ratio of the BET surface areas of the two electrodes, S_B/S_A = 232/98 = 2.4, suggesting that their surface compositions and structures were simi-

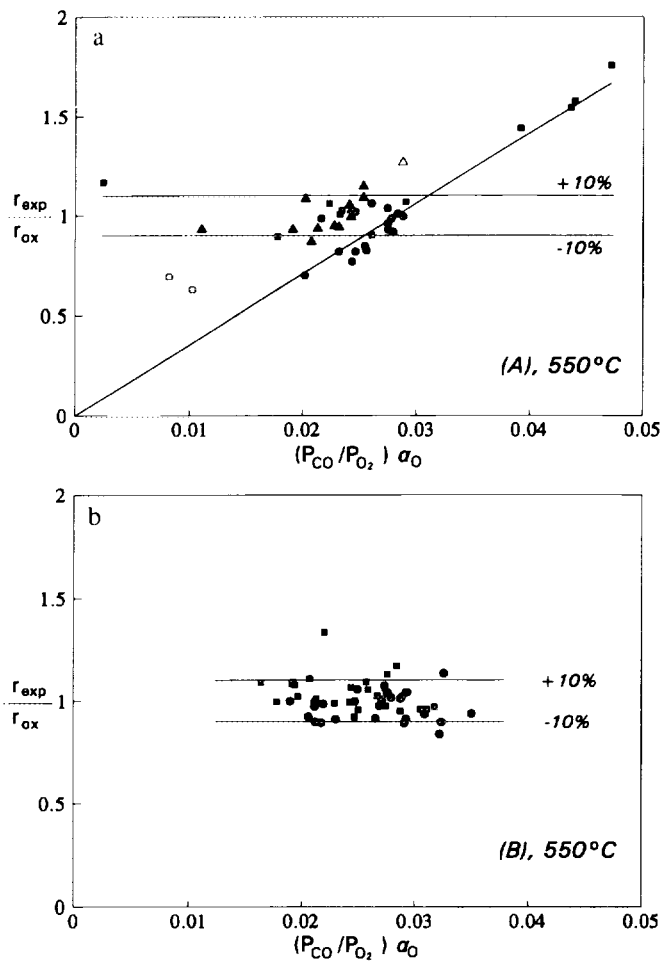

FIG. 10. The "error" of the reoxidation kinetics on the A-La(Sr)MnO_3 (a) and B-La(Sr)MnO_3 (b) catalysts at 550°C. Symbols are as in Figs. 8 and 9. The open symbols indicate data deviating from the predictions of the model.

lar. Accordingly, the reoxidation kinetic coefficient of $La_{0.5}Sr_{0.5}MnO_3$ catalyst would be

$$k_{ox} = 20.5(\pm 1.8) \times 10^{-2} \frac{\mu\text{mol}}{\text{s bar cm}^2}, \quad La_{0.5}Sr_{0.5}MnO_3\,(550°C). \quad [37]$$

The reduction coefficient of the catalyst can be estimated from the data on A-electrode to be

$$k_r = 3.0 \times 10^{-2} \frac{\mu\text{mol}}{\text{s bar cm}^2}, \quad \text{A-}La_{0.5}Sr_{0.5}MnO_3\,(550°C). \quad [38]$$

As predicted by the ionic redox model, the rate of the controlling step (reduction or reoxidation) can be determined by means of the catalyst oxygen activity. Accordingly, *given the reaction regime*, the multiple steady states can be described quantitatively. In most cases, the reaction was found to be reoxidation determined (Figs. 8, 9); this could be because the reaction of CO with r-oxygen is fast so that the exchange of oxygen between the bulk and the r-sites deviates from equilibrium. The rate can then be determined given the P_{O_2} and the α_O. The reaction was found to be reduction determined only when successive oxidizing treatments were employed, i.e., gas phase mixtures of $P_{O_2}/P_{CO} > 1$. The reaction regime cannot necessarily be determined given the catalyst oxygen activity and the gas phase composition. However, Fig. 10a suggests that the reaction could only be reoxidation determined at $\alpha_O \ll \alpha_O^*$ or reduction determined at $\alpha_O \gg \alpha_O^*$.

The Mars–van Krevelen Redox Model (500°C)

The rate of reaction at 500°C seems to be determined only by the gas phase composition. The oxygen activity, however, may show significant hysteresis, indicating that the rate does not depend on the oxidation state of the catalyst. This suggests that the reaction is limited to the surface of the catalyst and bulk oxygen species are not involved.

The rate measurements on both A- and B-La(Sr)MnO_3 electrodes can be estimated by Mars–van Krevelen kinetics, i.e., Eq. [29] in the linearized form,

$$\frac{P_{O_2}}{r} = \frac{1}{k_{ox}} + \frac{1}{k_r}\frac{P_{O_2}}{P_{CO}} \quad [39]$$

(A) $k_r = 1.68$, $k_{ox} = 3.92\ \mu\text{mol s}^{-1}\,\text{bar}^{-1}$

(B) $k_r = 2.74$, $k_{ox} = 15.9\ \mu\text{mol s}^{-1}\text{bar}^{-1}$.

In Figs. 11a and 11b plots of P_{O_2}/r against P_{O_2}/P_{CO} are presented for the electrodes A and B, respectively. Squares indicate measurements during O_2-cycles, while circles signify data obtained during CO-cycles. Solid lines indicate best fits. The reduction and reoxidation kinetic coefficients can be normalized by dividing by the surface areas of the two electrodes, to obtain

$$\begin{aligned} &\text{(A) } k_r = 1.7 \times 10^{-2}, \\ &\quad k_{ox} = 4.0 \times 10^{-2}\ \mu\text{mol s}^{-1}\,\text{bar}^{-1}\,\text{cm}^{-2} \\ &\text{(B) } k_r = 1.2 \times 10^{-2}, \\ &\quad k_{ox} = 6.9 \times 10^{-2}\ \mu\text{mol s}^{-1}\,\text{bar}^{-1}\,\text{cm}^{-2}. \end{aligned} \quad [40]$$

The kinetic measurements suggest that the reaction follows a Mars–van Krevelen redox mechanism at the surface of the catalyst,

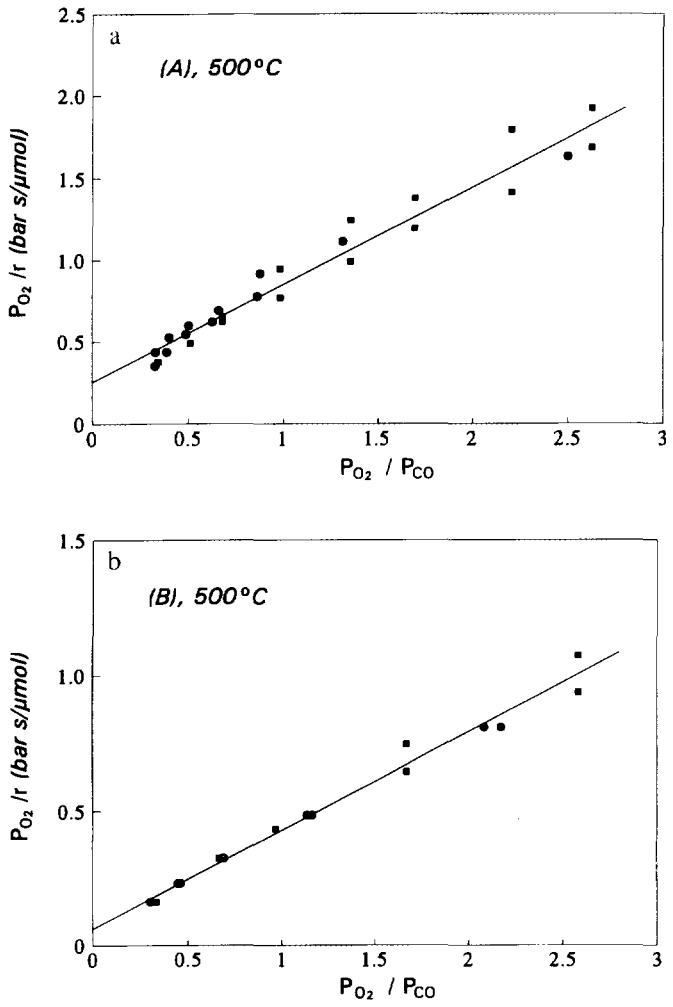

FIG. 11. Mars–van Krevelen kinetics on A-La(Sr)MnO_3 (a) and B-La(Sr)MnO_3 (b) catalysts at 500°C. Squares and circles signify the data during O_2- and CO-cycles, respectively.

$$O_2(g) + S \rightarrow O_2\text{–}S \qquad [41]$$

$$O_2\text{–}S + S \rightleftharpoons 2O\text{–}S \qquad [42]$$

$$CO(g) + O\text{–}S \rightarrow CO_2(g) + S. \qquad [43]$$

In this case, the reduced sites become reoxidized by gas phase oxygen and not through the oxide lattice. This should be because the overall lattice diffusion is inhibited, probably due to a decrease in the mobility of oxygen species. The change in the reaction mechanism may also be associated with a change in the active oxygen species.

Oxygen in the bulk is not in equilibrium with the surface species and accordingly the oxygen activity does not reflect the concentrations of the active species, i.e.,

$$K_O\alpha_O \neq \frac{\theta_{OS}}{\theta_S} = \frac{k_{ox}P_{O_2}}{k_rP_{CO}}. \qquad [44]$$

The concentration of oxygen in the bulk of the catalyst changes since the bulk interacts with the surface through the diffusion processes. The lack of equilibrium between the bulk and the surface, due to the low mobility of oxygen, causes the rate of the surface reaction to seem insensitive to changes in the oxidation state of the solid catalyst.

The kinetic model indicates that the kinetic coefficients of the two electrodes are different, i.e.,

$$k_r(A) > k_r(B), \quad k_{ox}(A) < k_{ox}(B). \qquad [45]$$

The above observation suggests that the surface compositions (or structures) of the two electrodes are different. This may be because of different bulk compositions; the oxygen activity measurements (Figs. 6 and 7) indicate that the A-La(Sr)$MnO_{3-\delta}$ electrode is in a "reduced" state, while the B-electrode is in an "oxidized" state,

$$\begin{aligned} A-&: 10^{-4}\,\text{bar}^{1/2} < \alpha_O < 10^{-3}\,\text{bar}^{1/2} \\ B-&: 10^{-2}\,\text{bar}^{1/2} < \alpha_O < 10^{-1}\,\text{bar}^{1/2}. \end{aligned} \qquad [46]$$

The kinetic coefficients of the surface reactions could then depend on the oxygen activity of the oxide catalyst. Multiple steady states may appear in the rate of reaction if significant changes in the oxidation state of the catalyst occur. The slight variations in the rate of reaction on A-La(Sr)MnO_3 (Fig. 6) could be associated with the transitions of the catalyst into substantially different oxygen content forms of La(Sr)$MnO_{3-\delta}$.

This effect could be viewed as a case of phase transition. If the oxygen activity regions of the two electrodes were much smaller than the difference between their mean values, then one could consider that different phases of the catalyst were effectively formed. This may be possible at a lower temperature, where the bulk oxygen concentration of the catalyst La(Sr)$MnO_{3-\delta}$ would not change significantly between different gas phase compositions. One could then reduce the catalyst at higher temperatures, create a different oxygen content form of La(Sr)$MnO_{3-\delta}$, and "freeze" it back at the original temperature. It is exactly because the communication between the surface and the bulk is limited that the two oxygen content forms of the nonstoichiometric oxide, δ and δ', could be considered as two different phases.

The Reaction Mechanism

The combination of kinetic and oxygen activity measurements during the CO oxidation on $La_{0.5}Sr_{0.5}MnO_{3-\delta}$ suggested that, in going from 500 to 550°C, the dominant reaction mechanism changes from a Mars–van Krevelen redox mechanism where the reoxidation of the reduced sites occurs by gas phase oxygen (500°C), to an ionic

redox mechanism where the reoxidation of the reduced sites occurs by lattice diffusion of oxygen species (550°C). The former reaction does not involve bulk lattice oxygen species, while the latter does. The transition seems to be associated with a change in the mobility of oxygen within the oxide lattice.

The TPD spectrum of oxygen from the $La_{0.5}Sr_{0.5}MnO_3$ suggested that the lattice oxygen species of the catalyst becomes mobile in the temperature range 500–550°C. Two oxygen peaks were present in the TPD spectrum (Fig. 1). The low-temperature peak (α-desorption) represents the desorption of surface oxygen species; its calculated coverage is approximately one monolayer. The high-temperature peak (β-desorption) involves the desorption of oxygen from the oxide bulk. The end of surface desorption and the onset of bulk desorption occur in the temperature range 500–550°C. The TPD spectrum in Fig. 1 is in excellent agreement with the TPD spectra on La(Sr)MnO_3 produced by other workers (14, 35, 36). Teraoka *et al.* (35) suggested that the onset temperature of bulk oxygen desorption of La(Sr)MnO_3 coincides with the thermal reduction temperature of Mn^{4+} to Mn^{3+}, namely 535°C. It should also be noted that Boreskov and Marshneva (37) suggested that the oxidation of CO on Mn_2O_3 follows the redox mechanism only at temperatures above 500°C.

The transition in the reaction mechanism may also be associated with a change in the active oxygen species. The fact that redox mechanistic models operate at both temperatures does not necessarily mean that lattice oxygen and vacancies are always the active surface species. As Bielanski and Haber (23) suggested, the redox equations describe both *suprafacial* and *intrafacial* reactions depending on the meaning attached to the oxidized O–S and reduced S sites. They may equally represent two different oxidation states of the same metallic cation.

Following the suggestion of Kasztelan (38) that only one electron transfer can occur in a redox reaction and, accordingly, only one electron-reduced site is formed on the catalyst surface, one may assume that the oxidized and reduced sites on the La(Sr)$MnO_{3-\delta}$ surface can be either Mn^{4+} ($Mn^{\cdot}_{Mn}$ in Kröger–Vink notation) and Mn^{3+} (Mn^{x}_{Mn}) or oxygen and vacancies associated with one electron, i.e., O^{-}_{O} ($O^{\cdot}_{O}$) and V^{-}_{O} ($V^{\cdot}_{O}$). At 500°C, the adsorption of gas phase oxygen may take place on the metal sites

$$O_2(g) + Mn^{3+} \rightarrow Mn^{4+} - O_2^- \qquad [47]$$

$$Mn^{4+} - O_2^- + Mn^{3+} \rightleftarrows 2\,Mn^{4+} - O^-. \qquad [48]$$

The diffusion of the O^- ions to the oxide lattice is inhibited; the CO will first adsorb and then react with the O^- species,

$$CO(g) + Mn^{4+} - O^- \rightarrow CO_2(g) + Mn^{3+}. \qquad [49]$$

At 550°C, conversely, the adsorption of oxygen may take place at oxygen vacancies on the catalyst surface (ox-sites),

$$O_2(g) + Mn - V^{-}_{O} \rightarrow Mn - O_2^- \qquad [50]$$

$$Mn - O_2^- + Mn - V^{-}_{O} \rightleftarrows 2\,(Mn - O^{-}_{O}). \qquad [51]$$

The ionic redox model suggests that the ox-species diffuse quickly to the lattice and the CO reacts with oxygen species generated from the bulk at the r-sites. The ox- and r-sites in the ionic redox mechanism could represent sites located at different regions of the catalyst surface and not necessarily different chemical sites; the oxygen adsorption and the CO reaction may then take place at spatially separated Mn/Mn* sites (39). The r-oxygen may be electron deficient surface lattice oxygen,

$$CO(g) + Mn^* - O^{-}_{O} \rightarrow CO_2(g) + Mn^* - V^{-}_{O}. \qquad [52]$$

The activation of the oxide lattice and the generation of the surface oxide ions, according to

$$O^{2-}_{b} + h^{\cdot} \rightarrow O^{-}_{O}, \qquad [53]$$

has been used to explain the high reactivity of p-type oxides (40, 41). The ionic redox model suggests that this oxide activation is determined by the diffusion of oxygen ions from the bulk to the surface. This is consistent with the fact that the oxide La(Sr)MnO_3 possesses a higher electronic (positive hole) than ionic conductivity.

The operating mechanisms of CO oxidation on oxides can be distinguished by means of the value of the apparent activation energy. It has been suggested (23, 37) that high activation energies ($E_a > 20$–24 cal/mol) are associated with intrafacial reactions, while low activation energies ($E_\alpha < 10$ cal/mol) indicate suprafacial reactions. The apparent activation energy of the reaction was determined in the range 500–550°C to be

$$E_a = 21 \pm 0.8 \text{ kcal/mol } La_{0.5}Sr_{0.5}MnO_3. \qquad [54]$$

This value is consistent with the transition of the reaction to an intrafacial mechanism in the temperature range 500–550°C.

Following the above interpretation, it may be possible for the change of the reaction mechanism from the Mars–van Krevelen redox mechanism (500°C) to the ionic redox mechanism (550°C) to be associated with a transition from a suprafacial to an intrafacial reaction.

CONCLUSIONS

The multiplicity of the steady state in oxide catalysis is often attributed to phase transitions of the solid catalyst.

This has been observed in catalytic systems such as CuO/Cu_2O/Cu (5, 29). This work suggests that multiplicity phenomena can be observed during carbon monoxide oxidation on the perovskite catalyst $La_{0.5}Sr_{0.5}MnO_{3-\delta}$ even when phase transformations do not take place. The investigation was performed at 500–550°C using solid electrolyte potentiometry to monitor *in situ* the oxygen activity (the oxidation state) of the solid catalyst.

At 550°C, the reaction rate and the oxygen activity of the catalyst exhibited simultaneously multiple steady states at constant gas phase compositions. The rate was found to be a function of the oxygen (or the carbon monoxide) partial pressure and the oxygen activity of catalyst. The results were explained by means of an ionic redox model, where the reoxidation and the reduction reactions occur at different sites on the catalyst surface. Oxygen is then transported through the oxide lattice from the ox-sites, where it is adsorbed, to the r-sites, where it reacts with CO. The hysteresis effect is attributed to diffusional limitations appearing during either the reoxidation of the r-sites or the reoxidation of the oxide bulk. In the former regime, the exchange of oxygen between the r-sites and the bulk deviates from equilibrium and the rate is determined based on the kinetics of the reoxidation reaction, $r = k_{ox}P_{O_2}/(1 + K_O\alpha_O)$ (reoxidation determined reaction). In the latter regime, it is the exchange of oxygen between the ox-sites and the bulk which deviates from equilibrium and the rate is determined based on kinetics of the reduction reaction, $r = k_rP_{CO}K_O\alpha_O/(1 + K_O\alpha_O)$ (reduction determined reaction). The hysteresis effect was very pronounced when transitions in the reaction regime occurred. The diffusional limitations causing the multiple steady states were considered to be a result of the competition between the surface reactions rather than a result of a low mobility of oxygen. In most cases, a reoxidation determined reaction was observed possibly because the reaction of CO with r-oxygen was fast and the "equilibrium" between the oxygen in the bulk and the r-sites was disturbed.

The diffusivity of oxygen in the oxide lattice decreased at lower temperatures, and the reaction mechanism was altered. At 500°C, the rate tended to depend only on the gas phase composition and not on the catalyst state. The reaction kinetics were described by a Mars–van Krevelen redox model, where the reoxidation of the reduced surface sites occurs by gas phase oxygen and not through the oxide lattice. Hysteresis appearing in the oxygen activity was attributed to the lack of synchronization between the bulk and the surface due to the low mobility of oxygen. The change of the reaction mechanism was supported by the oxygen TPD spectrum of the $La_{0.5}Sr_{0.5}MnO_3$ catalyst which, in excellent agreement with the results of other workers, showed that the lattice oxygen species becomes mobile in the temperature range 500–550°C.

ACKNOWLEDGMENTS

The State Scholarships Foundation (I.K.Y.) of Greece is gratefully acknowledged for financial support to P.D.P. We also thank Allied Signal for providing the zirconia thimbles.

REFERENCES

1. Stoukides, M., *Ind. Eng. Chem. Res.* **27,** 1745 (1988).
2. Lintz, H.-G., and Vayenas, C. G., *Angew. Chem. Int. Ed. Engl.* **28,** 708 (1989).
3. Vayenas, C. G., S. Bebelis, S., Yentekakis, I. V., and Lintz, H.-G., *Catal. Today* **11,** 303 (1992).
4. Breckner, E. M., Sundaresan, S., and Benzinger, J., *Appl. Catal.* **30,** 277 (1987).
5. Hildenbrand, H.-H., and Lintz, H.-G., *Appl. Catal.* **65,** 241 (1990).
6. Hildenbrand, H.-H., and Lintz, H.-G., *Catal. Today* **9,** 153 (1991).
7. Yao, Y. Y., *J. Catal.* **36,** 266 (1975).
8. Voorhoeve, R. J. H., Remeika, J. P., and Trimble, L. E., *Ann. N.Y. Acad. Sci.* **272,** 3 (1976).
9. Kuchynka, D. J., Cook, R. L., and Sammells, A. F., *J. Electrochem. Soc.* **138,** 1284 (1991).
10. Hammouche, A., Siebert, E., Hammou, A., Kleitz, M., and Caneiro, A., *J. Electrochem. Soc.* **138,** 1212 (1991).
11. Hammou, A., *Adv. Electrochem. Sci. Eng.* **2,** 87 (1993).
12. Kudo, T., and Fueki, K., "Solid State Ionics." Kodansha, Tokyo, 1990.
13. Voorhoeve, R. J. H., in "Advanced Materials in Catalysis" (J. J. Burton and R. L. Garten, Eds.), p. 129. Academic Press, New York, 1977.
14. Yamazoe, N., and Teraoka, Y., *Catal. Today* **8,** 175 (1990).
15. Tejuca, L. G., Fierro, J. L. G., and Tascon, J. M. D., *Adv. Catal.* **36,** 237 (1989).
16. Arai, H., Yamada, T., Eguchi, K., and Seiyama, T., *Appl. Catal.* **26,** 265 (1986).
17. Metcalfe, I. S., and Sundaresan, S., *AIChE J.* **34,** 195 (1988).
18. Lewis, B., and von Elbe, G., "Combustion, Flames and Explosions of Gases," 2nd ed., p. 71. Academic Press, London, 1961.
19. Petrolekas, P., Ph.D. thesis, Imperial College, London, 1994.
20. Baker, R. T., Metcalfe, I. S., Middleton, P. H., Petrolekas, P., and Steele, B. C. H., *in* "New Frontiers in Catalysis" (L. Guczi, F. Solymosi, and P. Tétényi, Eds.), p. 2127. Elsevier, Amsterdam, 1993.
21. Hammouche, A., Siebert, E., Kleitz, M., and Hammou, A., *in* "Proceedings, 1st International Symposium on Solid Oxide Fuel Cells" (S. C. Singhal, Ed.), Vol. 89-11, p. 265. The Electrochemical Society Inc., Pennington, NJ, 1989.
22. Mizusaki, J., Tagawa, H., Naraya, K., and Sasamoto, T., *Solid State Ionics* **49,** 111 (1991).
23. Bielanski, A., and Haber, J., "Oxygen in Catalysis." Dekker, New York, 1991.
24. Libre, J. M., Barbaux, Y., Grzybowska, B., Conflant, P., and Bonnelle, J. P., *Appl. Catal.* **6,** 315 (1983).
25. Ono, T., Nakajo, T., and Hironaka, T., *J. Chem. Soc. Faraday Trans.* **86,** 4077 (1990).
26. Kung, H. H., *J. Catal.* **134,** 691 (1992).
27. Mars, P., and van Krevelen, D., *Chem. Eng. Sci. Suppl.* **3,** 41 (1954).
28. Riekert, L., *Ber. Bunsenges. Phys. Chem.* **85,** 297 (1982).
29. Greger, M., Ihme, B., Kotter, M., and Riekert, L., *Ber. Bunsenges. Phys. Chem.* **88,** 427 (1984).
30. Hafele, E., and Lintz, H.-G., *Ber. Bunsenges. Phys. Chem.* **92,** 188 (1988).
31. Yentekakis, I. V., Neophytides, S., and Vayenas, C. G., *J. Catal.* **111,** 152 (1988).

32. Vayenas, C. G., Lee, B., and Michaels, J., *J. Catal.* **66,** 36 (1980).
33. Eng, D., Stoukides, M., and McNally, T., *J. Catal.* **106,** 342 (1987).
34. Balian, A., Hatzigiannis, G., Eng, D., and Stoukides, M., *J. Catal.* **145,** 526 (1994).
35. Teraoka, Y., Yoshimatsu, M., Yamazoe, N., and Seiyama, T., *Chem. Lett.*, 893 (1984).
36. Nitadori, T., Kurihara, S., and Misono, M., *J. Catal.* **98,** 221 (1986).
37. Boreskov, G. K., *Kinet. Katal.* **14,** 7 (1973); Boreskov, G. K., and Marshneva, V. I., *Dokl. Akad. Nauk SSSR* **213,** 112 (1973).
38. Kasztelan, S., *Ind. Eng. Chem. Res.* **31,** 2497 (1992).
39. Chan, K. S., Ma, J., Jaenicke, S., Chuah, G. K., and Lee, J. Y., *Appl. Catal.* **107,** 201 (1994).
40. Kazanskii, V. B., *Kinet. Katal.* **14,** 72 (1973).
41. Morrison, S. R., "The Chemical Physics of Surfaces." Plenum, New York, 1977.